Astronomy & Astrophysics

Magnetic variability in the young solar analog KIC 10644253

Observations from the *Kepler* satellite and the HERMES spectrograph

D. Salabert[1,2], C. Régulo[3,4], R. A. García[1], P. G. Beck[1], J. Ballot[5,6], O. L. Creevey[2], F. Pérez Hernández[3,4], J.-D. do Nascimento Jr.[7,8], E. Corsaro[1,3,4], R. Egeland[9,10], S. Mathur[11], T. S. Metcalfe[11], L. Bigot[2], T. Ceillier[1], and P. L. Pallé[3,4]

[1] Laboratoire AIM, CEA/DRF-CNRS, Université Paris 7 Diderot, IRFU/SAp, Centre de Saclay, 91191 Gif-sur-Yvette, France
e-mail: david.salabert@cea.fr
[2] Laboratoire Lagrange, Université Côte d'Azur, Observatoire de la Côte d'Azur, CNRS, Bd de l'Observatoire, CS 34229, 06304 Nice Cedex 4, France
[3] Instituto de Astrofísica de Canarias, 38200 La Laguna, Tenerife, Spain
[4] Departamento de Astrofísica, Universidad de La Laguna, 38205 La Laguna, Tenerife, Spain
[5] CNRS, Institut de Recherche en Astrophysique et Planétologie, 14 avenue Édouard Belin, 31400 Toulouse, France
[6] Université de Toulouse, UPS-OMP, IRAP, 31400 Toulouse, France
[7] Universidade Federal do Rio Grande do Norte, UFRN, Dep. de Física, DFTE, CP1641, 59072-970 Natal, RN, Brazil
[8] Harvard-Smithsonian Center for Astrophysics, Cambridge, MA 02138, USA
[9] High Altitude Observatory, National Center for Atmospheric Research, PO Box 3000, Boulder, CO 80307-3000, USA
[10] Department of Physics, Montana State University, Bozeman, MT 59717-3840, USA
[11] Space Science Institute, 4750 Walnut street Suite#205, Boulder, CO 80301, USA

ABSTRACT

The continuous photometric observations collected by the *Kepler* satellite over 4 yr provide a wealth of data with an unequalled quantity and quality for the study of stellar evolution of more than 200 000 stars. Moreover, the length of the dataset provides a unique source of information for detecting magnetic activity and associated temporal variability in the acoustic oscillations. In this regards, the *Kepler* mission was awaited with great expectations. The search for the signature of magnetic activity variability in solar-like pulsations still remained unfruitful more than 2 yr after the end of the nominal mission. Here, however, we report the discovery of temporal variability in the low-degree acoustic frequencies of the young (1 Gyr-old) solar analog KIC 10644253 with a modulation of about 1.5 yr with significant temporal variations for the duration of the *Kepler* observations. The variations agree with the derived photometric activity. The frequency shifts extracted for KIC 10644253 are shown to result from the same physical mechanisms involved in the inner subsurface layers as in the Sun. In parallel, a detailed spectroscopic analysis of KIC 10644253 is performed based on complementary ground-based, high-resolution observations collected by the HERMES instrument mounted on the *Mercator* telescope. Its lithium abundance and chromospheric activity $\mathcal{S}$ index confirm that KIC 10644253 is a young and more active star than the Sun.

Key words. stars: oscillations – stars: solar-type – stars: activity – methods: data analysis – methods: observational

1. Introduction

Photometric observations of the solar-like oscillator G0V KIC 10644253 (BD+47 2683, $V = 9.26$, [Fe/H] = 0.12 dex, and see Table 1) were collected continuously over four years between May 2009 and May 2013 by the *Kepler* satellite (Borucki et al. 2010). At first, its stellar properties were derived from grid-based modeling based on global seismic parameters combined with complementary photometry (Pinsonneault et al. 2012) and spectroscopy (Bruntt et al. 2012) as part of more than 500 solar-like *Kepler* targets (Chaplin et al. 2014). Because its effective temperature, above 6000 K (Bruntt et al. 2012), KIC 10644253 was part of the sample of 22 hot stars selected by Mathur et al. (2014a) when they reported a modulation in the temporal variation of its photometric magnetic activity. In the mean time, more precise stellar properties based on the fitted individual oscillation frequencies from Appourchaux et al. (2012) and derived using the Asteroseismic Modelling Portal (AMP; Metcalfe et al. 2014) substantially revised its mass downward by more than

20% to $1.13 \pm 0.05~M_\odot$ with an estimated age of 1.07 ± 0.25 Gyr. When making the best use of the asteroseismic observations, the stellar parameters of KIC 10644253 thus correspond to a solar analog, the youngest solar-like pulsating star observed by *Kepler* with a rotation period of 10.91 ± 0.87 days (García et al. 2014a). Furthermore, the unequalled length of the *Kepler* observations also provide a great opportunity to study stellar temporal variations by means of different observables, such as the surface magnetic activity (e.g., Frasca et al. 2011; Fröhlich et al. 2012; Bonanno et al. 2014a). Since the proxy for photometric magnetic activity suggests that KIC 10644253 is among the most active stars of the solar-like oscillators observed by *Kepler* (García et al. 2014a), and owing to its very solar-like fundamental stellar properties, KIC 10644253 is an excellent candidate for investigating the magnetic activity of a young Sun with asteroseismic data.

Indeed, it is well established that in the case of the Sun, acoustic (p) oscillation frequencies are sensitive to changes in the surface activity and that they vary in correlation with

Table 1. KIC 10644253 stellar properties.

Property	Value	Reference
Spectral type	G0 V	(1)
V	9.26 ± 0.02	(2)
$(B - V)$	0.59 ± 0.03	(2)
Mass ($M_\odot$)	1.13 ± 0.05	(3)
Radius R ($R_\odot$)	1.108 ± 0.016	(3)
Age (Gyr)	1.07 ± 0.25	(3)
R_{BCZ}/R	0.77 ± 0.03	(3)
$\upsilon \sin i_{spectro}$ (km s^{-1})	3.8 ± 0.6	(4)
T_{eff} (K)	6030 ± 60	(4)
$\log g$ (dex)	4.40 ± 0.03	(4)
[Fe/H] (dex)	0.12 ± 0.06	(4)
$\upsilon \sin i_{astero}$ (km s^{-1})	0.62 ± 0.81	(5)
ν_{max} (μHz)	2819 ± 131	(6)
$\Delta\nu$ (μHz)	123.6 ± 2.7	(6)
P_{rot} (days)	10.91 ± 0.87	(7)
$i_{spectro}$ (°)	48^{+11}_{-9}	(3+4+7)
i_{astero} (°)	7^{+9}_{-9}	(3+5+7)

References. (1) Molenda-Żakowicz et al. (2013); (2) Høg et al. (2000); (3) Metcalfe et al. (2014); (4) Bruntt et al. (2012); (5) Doyle et al. (2014); (6) Chaplin et al. (2014); (7) García et al. (2014a); (3+4+7) Derived from Metcalfe et al. (2014), Bruntt et al. (2012), and García et al. (2014a); (3+5+7) Derived from Metcalfe et al. (2014), Doyle et al. (2014), and García et al. (2014a).

activity proxies, such as the sunspot number or the 10.7 cm radio emission along the 11-yr solar cycle. Such temporal variations were quickly reported with the first helioseisimic observations by Woodard & Noyes (1985), and confirmed shortly thereafter by Fossat et al. (1987) and Libbrecht & Woodard (1990). As longer and higher-quality helioseismic observations became available, the temporal variability of the *p*-mode frequencies were studied in greater detail. These frequency shifts were actually observed to be frequency dependent, with larger shifts at higher frequencies, and to be angular-degree (*l*) dependent, i.e., mode-inertia dependent, although the *l* dependence is small for low-degree modes (see, e.g., Gelly et al. 2002; Howe et al. 2002; Jiménez-Reyes et al. 2004; Salabert et al. 2004). Moreover, Howe et al. (2002) showed that the temporal and latitudinal distribution of the frequency shifts is correlated with the spatial distribution of the surface magnetic field. The frequency shifts are explained as arising from indirect magnetic effects on the inner structural changes (Kuhn 1988; Dziembowski & Goode 2005) of the Sun along the solar cycle.

Today, solar frequencies are the only activity proxy that can reveal inferences on subsurface changes with solar activity not detectable at the surface by standard proxies (e.g., Salabert et al. 2009, 2015; Basu et al. 2012). Furthermore, a faster temporal modulation of the oscillation frequency variations with a period of about two years was observed to coexist in the Sun (Fletcher et al. 2010), which is believed to have an origin located deeper inside the convective zone. Except for the Sun, temporal variations of *p*-mode frequencies related to magnetic activity using asteroseismic techniques have so far been observed in only one star: the F5V star HD 49933 observed by the space-based Convection, Rotation, and planetary Transits (CoRoT, Baglin et al. 2006) satellite. Indeed, García et al. (2010) report for the first time that the acoustic oscillation parameters were varying in a comparable manner to the Sun and in correlation with the photometric measurements.

The frequency dependence of the activity-frequency relationship was also reported to be similar to the one observed in the Sun, but with larger shifts in accordance with a higher activity index (Salabert et al. 2011). Such asteroseismic inferences of the magnetic activity provide invaluable information when studying the physical phenomena involved in the dynamo processes in the interior of stars, and in this regards the four-year long continuous observations collected by the *Kepler* mission were awaited with great expectation for detecting activity cycles. The CoRoT target HD 49933 nonetheless remains the only object so far with the Sun where changes in the inner subsurface layers related to magnetic activity have been observed using asteroseismology.

Nevertheless, a large sample of stellar magnetic cycles covering a range between 2.5 and 25 yr were reported by several authors (e.g., Wilson 1978; Baliunas & Vaughan 1985; Baliunas et al. 1995; Hall et al. 2007) from spectroscopic measurements in the Ca II H and K emission lines at the Mount Wilson Observatory (MWO). Moreover, several authors have suggested that the periods of the activity cycles increase proportionally to the stellar rotational periods along two distinct paths in main-sequence stars: the active and the inactive stars (Saar & Brandenburg 1999; Böhm-Vitense 2007). Furthermore, nine stars with dual cycles were identified within the MWO survey (Baliunas et al. 1995), six of which made it into the refined sample of Saar & Brandenburg (1999), along with one newly reported dual-cycle star. Another 15 stars with multiple cycles were reported by Oláh et al. (2009) using photomometric and Ca II emission observations. Recently, Metcalfe et al. (2010) observed short-period variations of 1.6 yr on the exoplanet host star ι Horologi, and dual cycles of 2.95 and 12.7 yr, respectively, were found on ϵ Eridani, an exoplanet host star as well, by Metcalfe et al. (2013) with the high cadence SMARTS HK observations. Recently, Egeland et al. (2015) have observed Sun-like magnetic temporal variations in the G1.5V star HD 30495, a 1 Gyr-old solar analog with a rotation period of ∼11 days. They show that this star has short-period variations of ∼1.7 yr and a long modulation of ∼12 yr.

Another way to detect magnetic cycles is to directly measure the evolution of the photospheric magnetic field through the Zeeman effect. Activity cycles were found this way in late-type dwarf stars that exhibit a periodic polarity reversal of their magnetic field as observed in the Sun during its 11-yr cycle. For example, the F-type star τ Boo and HD 78366, rotating in 3.3 and 11.4 days, respectively, magnetic cycles of about two years (Fares et al. 2009) and shorter than three years (Morgenthaler et al. 2011) were observed. However, these periods can be different from the variations measured in chromospheric proxies: for instance, Baliunas et al. (1995) reported two periods of 5.9 and 12.2 yr in the chromospheric emission of HD 78366. It is then important to keep in mind that stellar magnetic activity cycles can be multiperiodic and that different varieties of observations provide complementary constraints on the underlying dynamo processes.

In that context, we investigate in this work the magnetic activity of the young solar analog KIC 10644253 by means of the photometric and high-resolution spectroscopic observations collected by the *Kepler* satellite and the HERMES instrument, respectively (Raskin et al. 2011; Raskin 2011). In Sect. 2, we describe the *Kepler* and HERMES data used in this paper. The methods applied to derive the photometric activity and the low-degree seismic acoustic frequencies, and the way the frequency shifts are estimated are described in Sect. 3. The results are presented and discussed in Sect. 4. In Sect. 5, the magnetic activity and age of KIC 10644253 are discussed in

Table 2. Journal of HERMES observations for KIC 10644253.

# spectrum	HJD (day)	Exposure time (s)	Radial velocity (km s^{-1})	$\mathcal{S}$	S/N(Ca)
1	2 457 087.68434	1600	-19.00 ± 0.04	0.207	27.9
2	2 457 087.77404	1700	-19.00 ± 0.04	0.221	38.2
3	2 457 088.71177	1800	-19.00 ± 0.04	0.213	16.5
4	2 457 088.73319	1800	-19.00 ± 0.04	0.243	21.5
5	2 457 090.73719	1600	-19.02 ± 0.04	0.248	34.4
6	2 457 090.75629	1600	-19.02 ± 0.04	0.221	33.7
7	2 457 130.72239	1800	-18.92 ± 0.04	0.209	38.9
8	2 457 163.60000	1600	-19.01 ± 0.04	0.219	30.3
9	2 457 189.62647	1600	-18.96 ± 0.04	0.204	38.2
10	2 457 215.45761	1600	-18.95 ± 0.04	0.214	31.6
11	2 457 241.48984	1000	-19.07 ± 0.04	0.207	25.3
12	2 457 267.39006	1000	-19.07 ± 0.04	0.226	24.2

Notes. The heliocentric Julian date (HJD) is given for the midpoint of each exposure. The $\mathcal{S}$-index values obtained for each individual spectrum are also reported. The S/N(Ca) in the range of the UV was calculated from the instrumental flux, corrected for the gain of the CCD at the centre of the 90th echelle order ($\sim$400 nm).

light of complementary spectroscopic HERMES observations. In Sect. 6, we provide interpretations of the inner structural changes of KIC 10644253 with activity and compare them to the Sun, while a summary of the results is given in Sect. 7.

2. Observations

Both the long-cadence (LC) and short-cadence (SC) observations[1] of KIC 10644253 collected by the *Kepler* satellite were used in this analysis. The LC data were analyzed over almost the entire duration of the mission from 2009 June 20 (Quarter 2, hereafter Q2) to 2013 May 11 (Q17; i.e., a total of about 1422 days). The two first quarters Q0 ($\sim$10 days) and Q1 ($\sim$33 days) were dropped because of calibration problems since it is performed quarter by quarter (see below). The light curve was corrected for instrumental problems using the *Kepler* Asteroseismic Data Analysis and Calibration Software (KADACS, García et al. 2011). The time series was then high-pass filtered with a triangular smooth function for periods longer than 55 days on a quarter-by-quarter basis. To reduce the effects of the regular gaps in the following analysis, all the gaps with a size smaller than 20 days were interpolated using an in-painting technique (for more details, see García et al. 2014b; Pires et al. 2015). With a sampling rate of 29.4244 min, the signature of the photospheric magnetic activity can be inferred by studying the temporal fluctuations of the light curve.

The SC data from Q5 (2010 March 20) to Q17 were used for the seismic analysis. Indeed, although 33 days of observations were collected during Q1, KIC 10644253 was not observed in SC during the three consecutive quarters Q2, Q3, and Q4. The SC sampling rate of 58.84876 s (Nyquist frequency of $\sim$8.50 mHz) is high enough to measure the low-degree p-mode oscillations centered on $\nu_{\max} = 2819 \pm 131 \mu$Hz (Chaplin et al. 2014). As for the LC data, the SC data were corrected using the KADACS pipeline, high-pass filtered with a triangular smooth function for periods longer than two days, and the gaps of sizes smaller than three days interpolated using the in-painting technique.

In addition to *Kepler* photometry, high-resolution spectroscopic observations of the solar analog KIC 10644253 were obtained in 2015 with the HERMES spectrograph, mounted to the 1.2 m *Mercator* telescope on La Palma (Canary Islands, Spain). Over a period of 180 days, 12 spectra were taken. The journal of observations is given in Table 2. The raw data were reduced with the instrument-specific pipeline (Raskin et al. 2011), thereby providing final data products that were rebinned to a constant resolving power of $R = 85\,000$ over the wavelength range in between 390 and 900 nm. The radial velocity for each individual spectrum was determined from a cross-correlation with the G2-mask in the HERMES pipeline toolbox. The radial velocity remains stable at -19.00 ± 0.04 km s^{-1}, which excludes the presence of a stellar companion given the 1σ night-to-night stability of 70 m s^{-1} of the HERMES spectrograph. Before combining the individual spectra through the median to a high signal-to-noise-ratio (S/N) spectrum, the spectra were normalized, utilizing a solar spectrum and shifted to the rest wavelength. The compiled median spectrum with an accumulated integration time of 5.2 h exhibits a S/N of $\sim$280 in the wavelength range corresponding to Strömgren y. Details about the post processing of the HERMES data can be found in Beck et al. (2016).

3. Measurement of the magnetic activity variability

3.1. Photometric magnetic activity proxy

The surface rotation period of stars can be measured from photometric observations due to the signature of the passage of spots inducing periodic modulations in the luminosity. Moreover, as shown by García et al. (2010) with the CoRoT observations of the F star HD 49933, the variability of the light curve, estimated by the standard deviation of the measurements and associated to the presence of spots or magnetic features rotating on the surface of the star, can be used as an index of stellar activity. However, because the variability in the light curves can have different origins and timescales (such as magnetic activity, convective motions, oscillations, stellar companion), the rotation period needs to be taken into account in calculating a magnetic activity index derived from the *Kepler* observations. In this way, most of the variability is only related to the magnetism (i.e., the spots) and not to the other sources of variability. Mathur et al. (2014b) showed that measuring the light curve fluctuations over subseries

---

[1] The Data Release 23 (DR23) short-cadence data were used in this analysis, and thus are not suffering from the calibration error recently discovered by the *Kepler*/NASA team, which only affects DR24.

of length $5 \times P_{\rm rot}$, where $P_{\rm rot}$ is the rotation period of the star in days, provides a good proxy for studying the temporal evolution of magnetic activity. A photometric index of stellar magnetic variability ($S_{\rm ph}$) can be thus derived from the *Kepler* observations. Salabert et al. (2016) show as well that such a photometric proxy can be directly applied to the solar observations, like the ones collected by the Variability of Solar Irrandiance and Gravity Oscillations (VIRGO; Fröhlich et al. 1995) photometric instrument onboard the Solar and Heliospheric Observatory (SoHO; Domingo et al. 1995) spacecraft. First of all, we used the entire duration of the *Kepler* observations up to Q17 to check that the surface rotation period of KIC 10644253 is consistent with the rotation of 10.91 ± 0.87 days reported by García et al. (2014a) using data up to Q14. The photometric activity proxy $S_{\rm ph}$ of KIC 10644253 was then calculated over 54.55-day-long subseries that overlapped by 6.82 days, using 1422 days of the continuous LC *Kepler* data from Q2 to Q17.

3.2. Extraction of the oscillation frequency shifts

To study the temporal variations of the low-degree *p*-mode oscillation frequencies, the SC *Kepler* dataset was split into contiguous 180-day-long subseries, overlapped by 30 days. We recall that as no observations of KIC 10644253 were collected during the quarters Q2, Q3, and Q4, we started the analysis from Q5 up to Q17. The quarter Q1 was disregarded because it is only 33 days long. A total of 34 non-independent 180-day subseries of a frequency resolution of about 0.06 μHz were thus analyzed with a mean duty cycle of 95%.

3.2.1. Cross-correlation analysis (Method #1)

The cross-correlation method returns a mean value of the frequency shift for all the visible modes in the power spectrum (Method #1). First introduced by Pallé et al. (1989) to measure the solar mean frequency shifts of the $l = 0, 1$, and 2 acoustic modes along the solar cycle from one single ground-based instrument, the cross-correlation method has since been widely used to study the temporal variation of the solar p modes from helioseismic observations (see Chaplin et al. 2007a, and references therein). More recently, the cross-correlation analysis was one of the methods employed to extract the frequency shifts of solar-like oscillations observed in a star other than the Sun, the F-type star HD 49933 observed by the CoRoT satellite (García et al. 2010).

The power spectrum of each 180-day subseries[2] was cross-correlated with a reference spectrum taken as the averaged spectrum of the independent spectra. The cross correlations were computed over five consecutive radial orders between 2480 μHz and 3080 μHz centered on the frequency of the maximum of the *p*-mode power excess (Chaplin et al. 2014). To estimate the frequency shift $\langle \delta \nu \rangle_{\rm Method\ \#1}$, the cross-correlation function was fitted with a Gaussian profile, whose centroid provides a measurement of the mean $l = 0, 1$, and 2 mode frequency shift over the considered frequency range. The associated 1σ uncertainties were obtained through Monte Carlo simulations as follows: the reference spectrum was shifted in frequency by the mean frequency shift obtained for each subseries; then 500 simulated power spectra were computed by multiplying the shifted reference spectrum by a random noise with a distribution following a χ^2 with two degrees of freedom. For each subspectrum, the

standard deviation of all the shifts obtained from the 500 simulated spectra with respect to the corresponding reference spectrum was adopted as the 1σ error bar of the fit (Régulo et al. 2016).

3.2.2. Mode peak-fitting analysis (Methods #2 and #3)

As explained in Sect. 3.2.1, the cross-correlation method returns a mean value of the frequency shift for all the visible $l = 0, 1$, and 2 modes in the power spectrum averaged over a given frequency range. The study of the frequency shifts estimated through the analysis of individual mode frequencies provide additional results using independent methods. To do so, the individual acoustic frequencies were measured using both a local (Method #2) and a global (Method #3) independent peak-fitting analysis as described below.

The power spectrum of each subseries of SC data was obtained in order to extract estimates of the *p*-mode oscillation parameters. The individual frequencies of the angular degrees $l = 0, 1$, and 2 provided by Appourchaux et al. (2012) were taken as initial guesses. The procedure for extracting the *p*-mode parameters was performed by fitting sequences of successive series of $l = 0, 1$, and 2 modes using a maximum-likelihood estimator as in Salabert et al. (2011) for the CoRoT target HD 49933 (Method #2). The individual $l = 0, 1$, and 2 modes were modeled using a single Lorentzian profile for each of the angular degrees l. Therefore, neither rotational splitting nor inclination angle were included in the fitting model. The height ratios between the $l = 0, 1$, and 2 modes were fixed to 1, 1.5, and 0.5, respectively, as for the ones typically expected for *Kepler* stars (Ballot et al. 2011a), and only one linewidth was fitted per radial order n. The natural logarithms of the mode height, linewidth, and background noise were varied, resulting in normal distributions. The formal uncertainties in each parameter were then derived from the inverse Hessian matrix. The mode frequencies thus extracted were checked to be consistent within the 1σ errors with Appourchaux et al. (2012). Additionally, we analyzed the temporal variations of the mode amplitudes and linewidths as they are known to vary with magnetic activity in the Sun (see, e.g., Chaplin et al. 2000; Salabert & Jiménez-Reyes 2006), but the results are not reliable because of a poor determination of these parameters at the level of precision of the data.

Alternatively, we also used a global peak-fitting technique to derive the mode parameters (Method #3). We used the procedure described in Ballot et al. (2011b) in which the power spectrum is modeled as the sum of a background noise and oscillation modes. The background noise was described by an Harvey profile, and each mode of a given angular degree l and radial order n was modeled as multiplets of Lorentzian profiles parametrized by a central frequency, a height, a linewidth, a rotational splitting (common to all modes), and an inclination angle. We considered modes of degree $l = 0, 1$, and 2 and 11 consecutive radial orders. To reduce the parameter space, the height ratios were fixed to 1, 1,5, and 0.5, respectively, and one linewidth was fit per radial order like in Method #2. All the parameters were estimated by performing a maximum a posteriori estimation (e.g., Gaulme et al. 2009). This procedure was individually applied to each 180-day power spectrum.

The mean temporal variations of the frequencies were defined as the differences between the frequencies observed on different dates and reference values of the corresponding modes. The set of reference frequencies was taken as the average over the entire observations. The frequency shifts $\langle \delta \nu \rangle_{\rm Method\ \#2}$ and $\langle \delta \nu \rangle_{\rm Method\ \#3}$ thus obtained were then averaged over

---

[2] The *Kepler* SC time series was first transformed into a regular temporal grid.
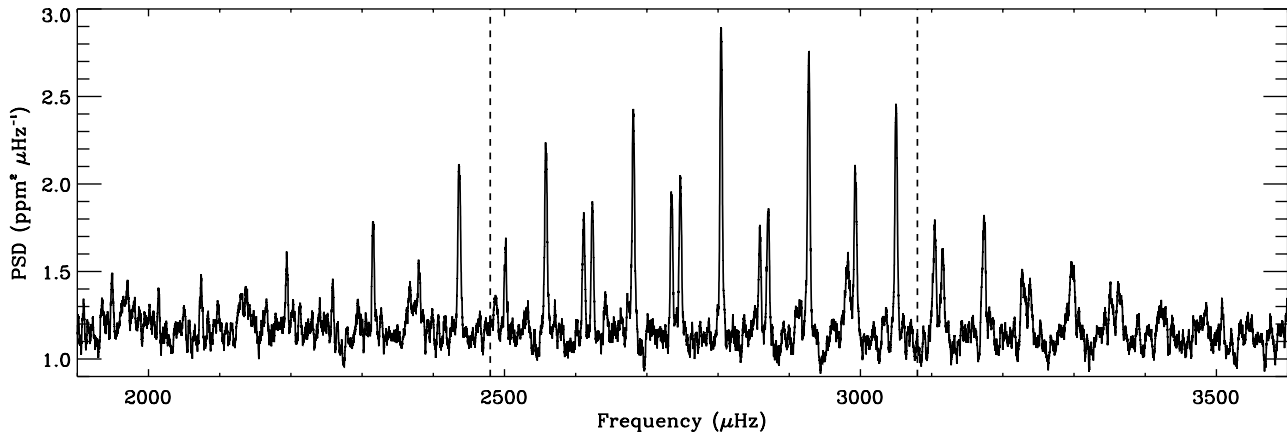
Fig. 1. Power spectrum of KIC 10644253 observed by the *Kepler* satellite centered on the frequency range of the measured acoustic oscillations and obtained by averaging the analyzed 180-day power spectra having a duty cycle higher than 80% and smoothed over 4 μHz. The vertical dashed lines indicate the frequency range chosen for analyzing the frequency shifts.

five consecutive radial orders between 2480 μHz and 3080 μHz, i.e. the same frequency range as the one used for the cross-correlation analysis in Sect. 3.2.1. The frequency range was currently defined by the lowest and highest modes, which were accurately fit in all the analyzed 180-day power spectra. Because the cross-correlation method returns mean frequency shifts unweighted over the analyzed frequency range, we decided to use unweighted averages of the frequency shifts extracted from the individual frequencies. We also note that we did not use the frequencies of the $l = 2$ mode because of its lower signal-to-noise ratio.

We also tried to extract the temporal variation of the amplitude of the *p*-mode envelope from the 180-day power spectra in the same manner as for HD 49933 (García et al. 2010) using the A2Z pipeline (Mathur et al. 2010). Indeed, the amplitudes of solar-like oscillations in stars were observed to be suppressed with magnetic activity (e.g., Mosser et al. 2009; García et al. 2010; Chaplin et al. 2011; Bonanno et al. 2014b). However, the absolute values of the oscillation amplitudes in the *Kepler* observations are subject to intrinsic changes due to the rotation of the satellite by 90° every three months. The consequence of this procedure is that a given target is observed with a different aperture in each of the CCDs, which have their own sensitivity and sources of noise as well. For these reasons, we were unable to extract reliable temporal evolution of the amplitude of the modes.

4. Results

The power spectrum of KIC 10644253 averaged over the analyzed 180-day *Kepler* power spectra and centered between 1900 and 3600 μHz around its maximum oscillation power is shown on Fig. 1. We recall here that the frequency resolution is about 0.06 μHz. For illustrative purpose, the spectrum was smoothed over 4 μHz. The LC data of KIC 10644253 over the full duration of the *Kepler* mission of about four years is represented in the top panel of Fig. 2, where the periodic modulation corresponds to the passage of spots. The middle panel shows the mean frequency shifts of the visible low-degree modes as a function of time obtained from the cross-correlation analysis (Method #1) of the SC data using 180-day non-independent subseries. The frequency shifts are compared to the photometric activity proxy, S_{ph}, estimated from the LC data (see Sect. 3.1). The bottom panel of Fig. 2 shows the frequency shifts of the individual angular degrees $l = 0$ (triangles) and $l = 1$ (circles) extracted

from the local peak-fitting analysis (Method #2) using the same data as in Method #1, which are also compared to the photometric activity proxy S_{ph}. We note that comparable results within the error bars are obtained from the global peak-fitting analysis (Method #3), but for illustrative purpose, we only show the results from Method #2.

The photometric activity proxy, S_{ph}, shows temporal variations going from periods of low activity (~300 ppm) to periods of higher activity (~1200 ppm) with clear rising and declining phases and a mean value of 549.4 $\pm$ 13.3 ppm. For comparison, the mean value of the photometric activity level of the Sun estimated from the VIRGO observations is $S_{ph,\odot} = 172.58 \pm 0.43$ ppm with values of $S_{ph,MAX\odot} = 255.37 \pm 0.62$ ppm and $S_{ph,MIN\odot} = 65.91 \pm 0.23$ ppm, respectively, at the maximum and minimum of the solar activity (Salabert et al. 2016). The *p*-mode frequency shifts of KIC 10644253 are also observed to vary with time with a comparable modulation with a minimum-to-maximum swing of about 0.5 μHz. The three independent methods return consistent variations of the frequency shifts within the precision of the measurements. The cross-correlation method (Method #1), however, returns smaller frequency shifts than the ones obtained from the peak-fitting analysis (Methods #2 and #3). This can be explained by the fact that the frequency shifts extracted from the cross-correlation method (Method #1) correspond to a mean shift over the entire analyzed frequency range and not only of the individual mode frequencies as in Methods #2 and #3. Moreover, our results show that the individual $l = 0$ and $l = 1$ frequency shifts show similar variations, although the $l = 0$ frequency shifts present a larger scatter, which translates into larger errors. This is probably due to the interplay with the nearby lower signal-to-noise ratio $l = 2$ modes with a different surface weight. Furthermore, the frequency shifts, which are related to the response of magnetic and structural changes inside the star, are observed to increase before the surface photometric activity proxy does. Indeed, the rising phase in the frequency shifts is observed to start about 100 days before, while both observables appear to be more in phase during the falling phase of the modulation. We note that in the case of the Sun, time delays of about 60−90 days between the low-degree frequency shifts and the surface activity proxies were observed as well (Salabert et al. 2009, 2013).

Lomb-Scargle (LS) periodograms were calculated from both the frequency shifts of the $l = 0$ and $l = 1$ modes and also from the photometric activity proxy using only independent
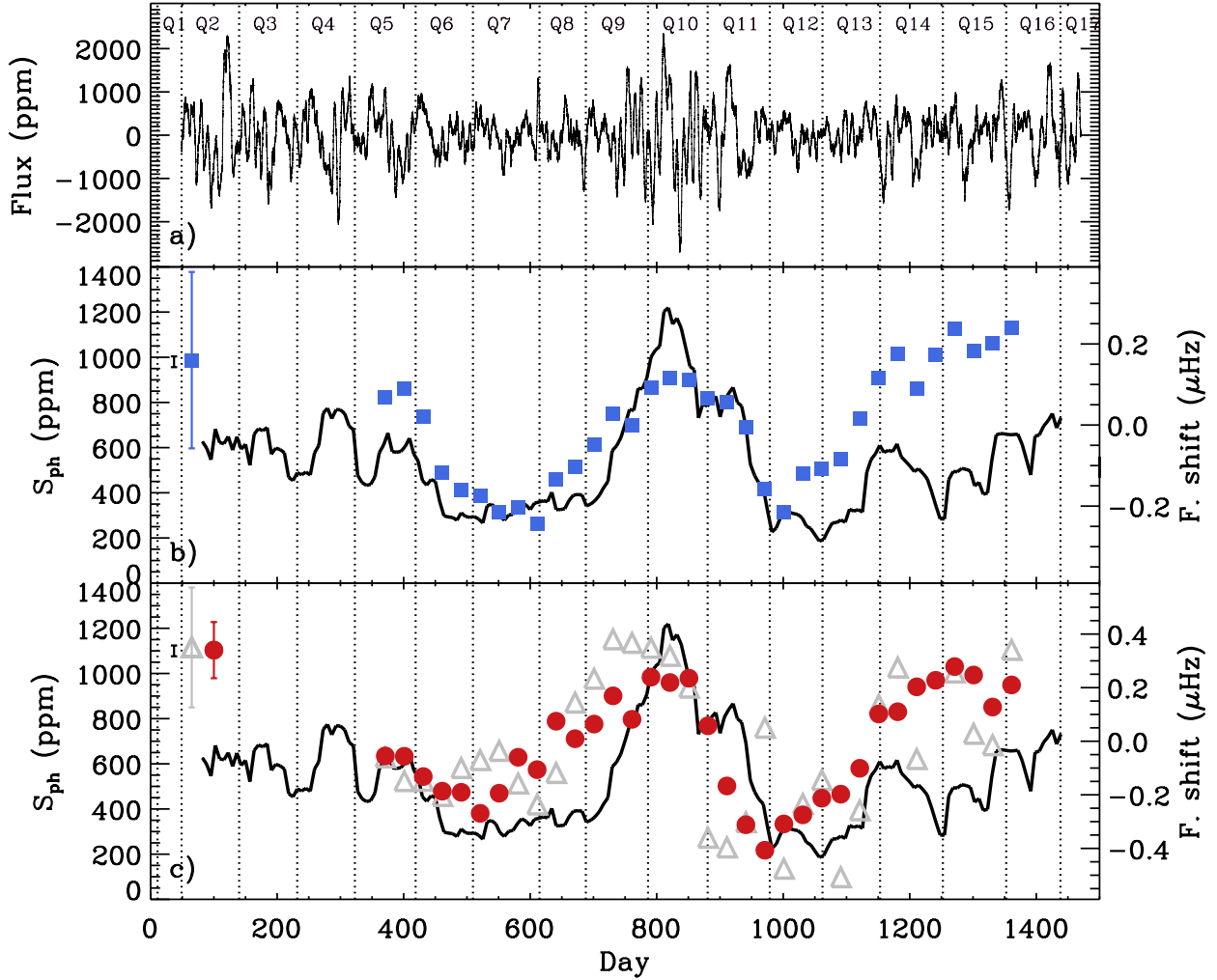
Fig. 2. *Top panel*: Q2 to Q17 photometric long-cadence observations (in ppm) of KIC 10644253 collected over 1422 days by the *Kepler* satellite as a function of time. *Middle panel*: magnetic activity photometric proxy S_{ph} (in ppm, black line) of KIC 10644253 estimated from the long-cadence observations as a function of time compared to the mean frequency shifts of the visible modes obtained from the cross-correlation analysis (Method #1, in μHz, blue squares). The frequency shifts were extracted from the continuous short-cadence observations from Q5 to Q17. *Bottom panel*: same as the middle panel but for the frequency shifts of the individual angular degrees $l = 0$ (gray triangles) and $l = 1$ (red circles) extracted from the local peak-fitting analysis (Method #2). The associated mean uncertainties are illustrated in the upper lefthand corner of each panel using the same color/symbol code. In the three panels, the vertical dotted lines represent the observational length of each *Kepler* quarter from Q0 to Q17.

Table 3. Most significant period (P_{max}) in days in the Lomb-Scargle periodograms calculated from the photometric activity proxy (S_{ph}) and the frequency shifts, $\langle \delta \nu \rangle$, extracted from the three independent methods.

Observable	P_{max} (day)	FAP
S_{ph}	582	0.05
$\langle \delta \nu \rangle_{\text{Method \#1}}$	514	0.52
$\langle \delta \nu_{l=1} \rangle_{\text{Method \#2}}$	514	0.43
$\langle \delta \nu_{l=1} \rangle_{\text{Method \#3}}$	514	0.64
$\langle \delta \nu_{l=0} \rangle_{\text{Method \#2}}$	600	0.68
$\langle \delta \nu_{l=0} \rangle_{\text{Method \#3}}$	600	0.67

Notes. The associated false alarm probability (FAP) are also given. Only independent points were used.

points (Fig. 3). We note that the LS periodograms were obtained by applying a four-time oversampling. The returned most significant periods and FAPs are given in Table 3, including the ones obtained from the three methods used to extract the frequency shifts. The periodograms in Fig. 3 show a significant

period centered on ∼550 days, i.e. ∼1.5 yr, given the resolution of the data. This period is comparable to the mean short-period variations of ∼1.7 yr found by Egeland et al. (2015) in the young 1 Gyr-old G1.5V solar analog HD 30495, which has a similar surface rotation period of 11.3 days and a long-period activity cycle of 12 yr. They used a windowed Lomb-Scargle analysis to determine both quasi-periodic and intermittent variations over the 48-yr period of the MWO observations, with the period of the variations ranging from ∼1.2 to ∼2.5 yr. However, as explained by Egeland et al. (2015), the short-period variation in HD 30495 was somewhat difficult to pin down. By comparison with KIC 10644253, the ∼1.5-yr variation also appears to be intermittent in the photometric activity proxy S_{ph}, with one strong oscillation centered on day 850 (Fig. 2). Furthermore, this object has very comparable stellar properties to KIC 10644253, including the surface rotation period. In addition, values reported by Egeland et al. (2015) are remarkably close to the two mean variations observed in the Sun's activity: the 11-yr cycle and the quasi-biennial oscillation (QBO; see, e.g., Bazilevskaya et al. 2014, and references therein). Moreover, the solar QBOs observed in various activity proxies are
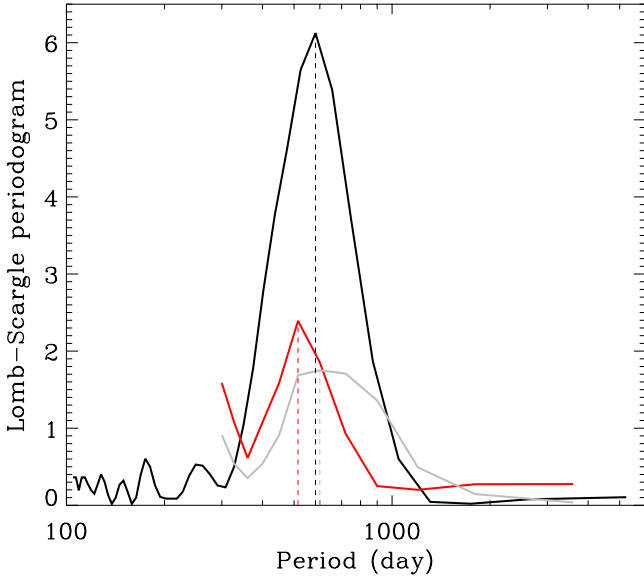
Fig. 3. Lomb-Scargle periodograms of the photometric activity proxy S_{ph} (black) and of the frequency shifts of the individual $l = 0$ (gray) and $l = 1$ (red) modes extracted from the analysis of KIC 10644253 using Method #2. Only independent points were used. The vertical dashed lines correspond to the associated maximum of the periodograms.
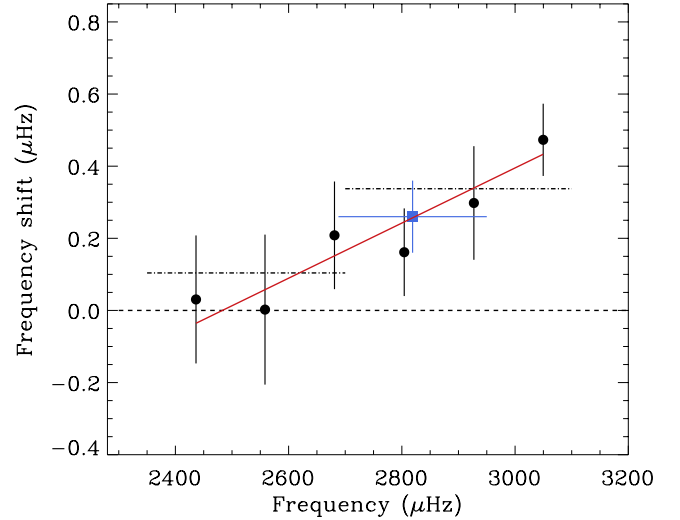

Fig. 4. Frequency shifts of the individual $l = 1$ frequencies (black dots) of KIC 10644253 as a function of frequency. The dot-dashed lines correspond to the weighted averages over two different frequency ranges represented by the total length of the lines, while the red solid line corresponds to a weighted linear fit. The blue square corresponds to the modeled value of the frequency shift at ν_{max} (see Sect. 6 and Table 1).

Table 4. Mean $l = 1$ frequency shifts of KIC 10644253 over two frequency ranges obtained from the individual frequencies (Method #2) extracted between two periods of high and low activity.

$\langle \delta\nu \rangle_{\text{Method \#2}}$	Frequency range (μHz)	
	[2350–2700]	[2700–3100]
$l = 1$	0.10 ± 0.31	0.34 ± 0.22

also characterized by intermittence in periodicity and with amplitudes that vary with time, which are larger around times of solar activity maxima. A tempting and simple hypothesis that one can speculate about for the solar analog KIC 10644253 is that the ~1.5-yr variation observed here in the photometric activity proxy and the oscillation frequency shifts is actually the signature of the short-period modulation, or QBO, of its magnetic activity as observed in the Sun (see, e.g., Fletcher et al. 2010; Broomhall et al. 2012; Simoniello et al. 2013) and the 1-Gyr-old solar analog HD 30495 (Egeland et al. 2015). We note, however, that in the case of the Sun, the frequencies shifts of the low-degree p modes between minimum and maximum of the 11-yr solar cycle vary by about 0.4 μHz and by about 0.1 μHz over the QBO period. Longer observations are still needed to confirm the analogy of the activity temporal variations measured in KIC 10644253 with the ones observed by Egeland et al. (2015) in HD 30495 and in the Sun (Bazilevskaya et al. 2014).

The frequency shifts of the solar p modes are also observed to follow an inverse mode-mass scaling (Libbrecht & Woodard 1990), which is explained as arising from changes in the outer inner layers, with larger variations observed in the high-frequency modes than in the low-frequency modes (e.g., Libbrecht & Woodard 1990; Chaplin et al. 1998; Salabert et al. 2004). Such a frequency dependence has only been observed today in one star other than the Sun, the F star HD 49933 (Salabert et al. 2011). Broomhall et al. (2012) report as well a frequency dependence of the solar QBO, although it is weaker than the frequency dependence along the 11-yr solar cycle. From the Fig. 5 in Broomhall et al. (2012), we can estimate that the ratio is roughly of about a factor 3. To detect any possible frequency dependence in the frequency shifts observed here for the solar analog KIC 10644253, oscillation mode frequencies were extracted over two periods of lower and higher activity in the same manner as described in Sect. 3.2.2 (Method #2) for six consecutive radial orders between 2350 and 3080 μHz. The frequency shifts at each radial order were thus obtained by simply

subtracting the frequencies measured during high activity by the corresponding frequencies at low activity. We only considered the $l = 1$ modes, because the $l = 1$ frequencies present the most significant swing between high and low activity over the entire epoch considered here. The results are shown in Fig. 4, where we see that the modes at higher frequency are more shifted than the ones at low frequency, reaching a maximum of about 0.5 μHz for the highest analyzed radial order. The mean frequency shifts over two different frequency ranges and weighted by using the formal errors are also represented and given in Table 4. This frequency dependence closely resembles what is already observed for the Sun and the F star HD 49933: higher shifts at higher frequencies.

Furthermore, there is strong evidence that fast-rotating young active stars show long-lived spots compared to the rotation period. As described in Lanza et al. (2014), the decay of the auto-correlation of the light curve can provide information on the lifetime of the active regions in a model-independent way. We found that the spot pattern in KIC 10644253 is observed to live around ~300 days, hence a lifetime that is much longer than the surface rotation of 10.9 days. Moreover, regarding the potentiality of studying possible evidence of differential rotation, Aigrain et al. (2015) demonstrate with a blind hare-and-hounds exercise that all the existing methods developed today to extract the differential rotation in stars are not yet fully reliable. For these reasons, such an analysis was not performed here, because further developments will be required to validate these methods.
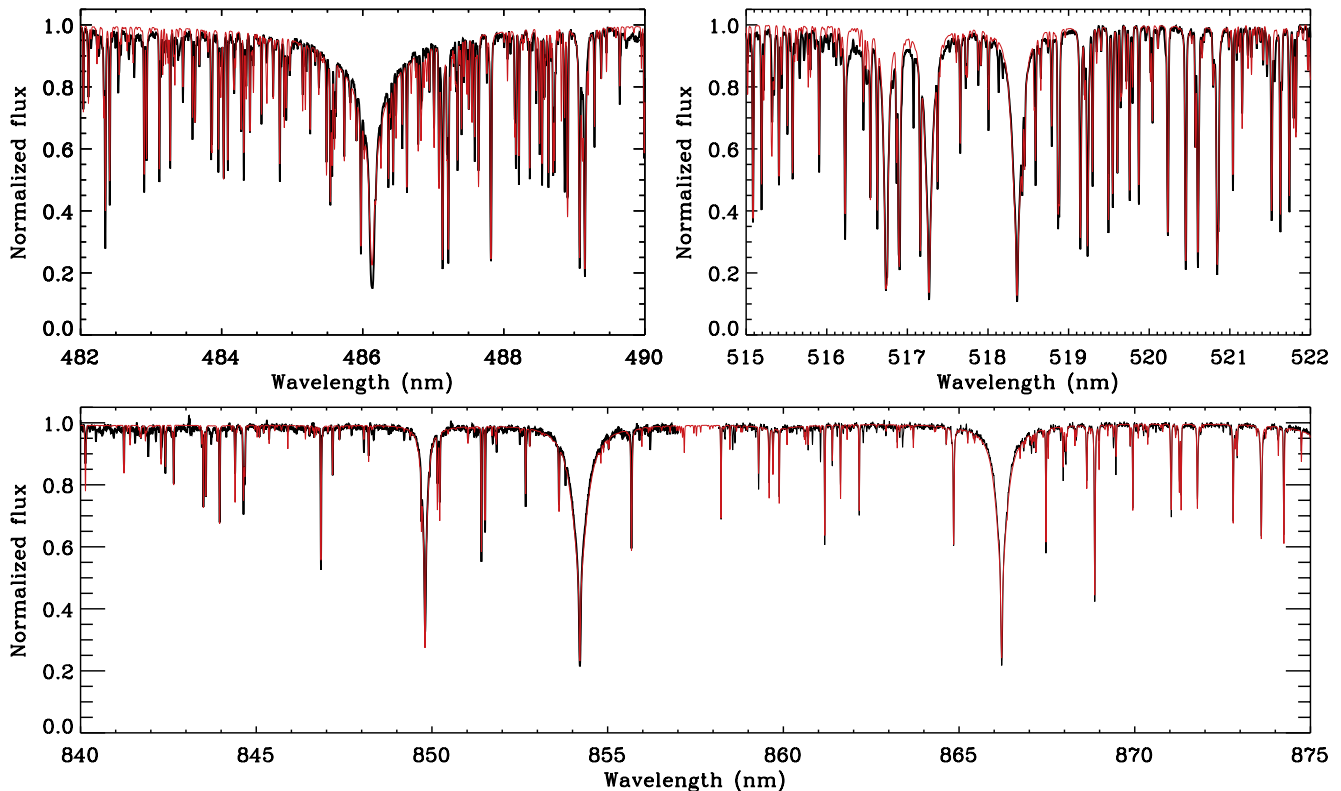
Fig. 5. Examples of the normalized spectrum of KIC 10644253 (in black) collected by the HERMES spectrograph over three different wavelength ranges, respectively around the lines H$_\beta$ (*top-left panel*), Mg II (*top-right panel*), and the Ca IRT triplet (*bottom panel*). The associated best fitting synthetic spectra are represented in red.

5. Spectroscopic analysis

The combined spectrum of KIC 10644253 has an extremely high S/N (~280), allowing us to perform a detailed spectroscopic analysis. In Fig. 5, the observed spectrum is shown around the H$_\beta$ line at 486 nm, as well as the lines Mg II 518 nm and Ca-triplet in the near infrared around 850 nm. These lines are particularly sensitive to the fundamental parameters. The lines needed for the elaborated spectral analysis of the lithium content, as well as the chromospheric activity as discussed below, are shown in Fig. 6 and compared to the solar spectrum.

5.1. Chromospheric activity

The stellar activity level can be quantified through the $\mathcal{S}$ index (Duncan et al. 1991, and references therein), which measures the strength of the emission in the cores of the Ca II H and K lines in the near UV. The lefthand panel of Fig. 6 compares the central region of the Ca K line in KIC 10644253 to the solar spectrum obtained with HERMES in April 2015 (Beck et al. 2016). The instrumental factor to scale the $\mathcal{S}$ index derived with HERMES into the MWO system is $\alpha = 23 \pm 2$ (Beck et al. 2016). It was estimated using observations collected with the HERMES spectrograph of G2-type stars from the Mount Wilson Observatory archive (MWO, Duncan et al. 1991).

The $\mathcal{S}$ index was estimated from the unnormalized but order-merged individual spectra and converted into the MWO system. For each spectrum, the corresponding value is reported in Table 2. The associated mean $\mathcal{S}$ index is $\mathcal{S} = 0.219 \pm 0.014$ (Table 5). Over the 180-day time base of the HERMES monitoring and given the few observed data points, the $\mathcal{S}$ index can

be considered to remain stable within the 1σ dispersion of the measurements quoted as the error on the mean value. Comparing this value to the activity level of the Sun during its active phase of cycle 24, $\mathcal{S}_\odot = 0.180$ (Beck et al. 2016) and represented in Fig. 6, we can estimate that KIC 10644253 is at least 20% more active than the Sun. This agrees with what can be expected for young active stars with observed p-mode oscillations, while such young stars with no pulsations can be much more active than KIC 10644253 (e.g., Frasca et al. 2011; Fröhlich et al. 2012). However, since we have no indication of the phase of the activity modulation when the HERMES observations were taken, this number could actually be even larger at maximum of activity. It is also worth mentioning that the high-resolution spectropolarimetric BCool survey (Marsden et al. 2014) measures surface magnetic fields and chromospheric activity proxies of cool solar-type stars. They show that magnetic fields are likely to be detected for stars with a $\mathcal{S}$ index greater than about 0.2, which is the case for KIC 10644253.

The Mount Wilson $\mathcal{S}$ index is however affected by line blanketing in the continuum regions near the H and K lines, which biases the value for less massive stars. To correct for this, another dimensionless ratio R'_{HK} was proposed in Noyes et al. (1984), which applies a correction factor for the line blanketing and attempts to remove the photospheric contribution to the line core using an empirically derived relationship. The log R'_{HK} is frequently used throughout the literature and is more appropriate for comparing the chromospheric activity of KIC 10644253 to the Sun. Using the mean $\mathcal{S} = 0.213$ and the $(B - V) = 0.59$ (see Table 1) with the Noyes et al. (1984) relationships, we obtained log $R'_{HK} = -4.720 \pm 0.045$. The uncertainty in log R'_{HK} was derived using standard error propagation methods. This again
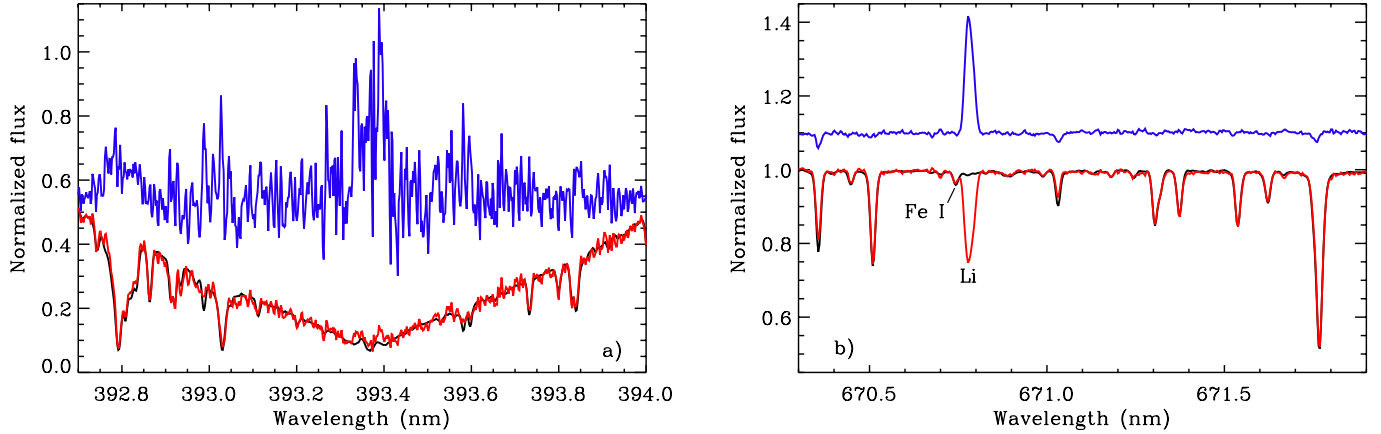
Fig. 6. Comparison of the solar spectrum (black) to the spectrum of the solar analog KIC 10644253 observed with the HERMES spectrograph. The regions around the Ca K line and the lithium multiplet at 670.78 nm are respectively shown in the *left and right panels*. The flux ratio (blue) of the two spectra between KIC 10644253 and the Sun (*left*), and between the Sun and KIC 10644253 (*right*) are also shown after shifting them by −0.45 and +0.1 respectively.

shows that KIC 10644253 is more active than the Sun, whose $\log R'_{\rm HK}$ value ranges from −4.86 to −4.95 from solar maximum to minimum (Hall et al. 2007).

5.2. Fundamental parameters and lithium abundance

To determine the fundamental parameters of KIC 10644253, we performed a grid search by comparing the observed spectrum to a library of synthetic spectra, which were computed using the SYNTHV radiative transfer code (Tsymbal 1996) based on the precomputed grid of atmosphere models from the LLMODELS code (Shulyak et al. 2004). The search was based on a 40 nm-wide wavelength range, containing the H_β and the Mg-triplet lines, as well as a ~35 nm-wide range containing the Ca infrared triplet at 860 nm, using the *Grid Search in Stellar Parameters* (GSSP[3]) software package (Lehmann et al. 2011; Tkachenko et al. 2012; Tkachenko 2015). The estimated effective temperature ($T_{\rm eff} = 6006 \pm 100$ K) and the surface gravity ($\log g = 4.3 \pm 0.1$ dex) are in excellent agreement with the results from Bruntt et al. (2012). However, the metallicity reported by Bruntt et al. (2012) of [Fe/H] = 0.12 ± 0.03 dex differs from the value of 0.2 ± 0.1 dex found here, but the difference falls within the quoted error of 0.1 dex. The summary of the results obtained from the analysis of the HERMES observations is given in Table 5, while the comparison between the observed and synthetic spectra is shown in Fig. 5.

Following do Nascimento et al. (2013), the lithium abundance of KIC 10644253 was derived from the Li I resonance transition at 670.7 nm by producing and comparing a synthetic spectrum to the observed HERMES spectrum for the set of atmospheric parameters given in Table 5, to match a single-line equivalent width. This procedure requires an atmosphere model and physical parameters of a list of absorption lines to compute atomic chemical abundances. The atmosphere models were interpolated in the Kurucz grid (Kurucz 1993) and the synthetic spectra were calculated with the MOOG routine by Sneden (1973). We note that the default solar abundances used here were taken from Anders & Grevesse (1989).

Table 5. Summary of the results obtained from the analysis of the HERMES spectroscopic observations of KIC 10644253.

Time base (days)	180
Mean radial velocity (km s^{-1})	−19.00 ± 0.04
$T_{\rm eff}$ (K)	6006 ± 100
$\log g$ (dex)	4.3 ± 0.1
[M/H] (dex)	0.2 ± 0.1
$v \sin i$ (km s^{-1})	1 ± 2
A(Li) (dex)	2.74 ± 0.03
S	0.219 ± 0.014
$\log R'_{\rm HK}$	−4.691 ± 0.059

The lithium abundance[4] of KIC 10644253 was derived to be A(Li) = log N(Li) = 2.74±0.03 dex, which agrees with the value of Bruntt et al. (2012) of A(Li) − A(Li)$_\odot$ = 1.74, for a solar abundance A(Li)$_\odot$ = 0.96 (Ghezzi et al. 2009). The detailed modeling of the resonance doublet, composed of the lines of ^{7}Li and ^{6}Li at 670.7754 and 670.7766 nm, respectively, is shown in Fig. 7. The main sources of error on the Li abundance are related to the uncertainties on the stellar parameters and equivalent-width measurement, however $T_{\rm eff}$ is by far the dominant source of error. The lithium abundance of 2.74 dex and a rotation period around 10.9 days are consistent with a young star, because stars in the Praesepe and Hyades clusters as determined by Soderblom et al. (1993). The two clusters are believed to be younger than 0.6 Gyr old. The rotation period is also consistent with the one obtained for 1.1 solar-mass stars of the 1 Gyr-old cluster NGC 6811 as described by Meibom et al. (2011). This result suggests that KIC 10644253 is a young object based on its Li depletion history (Ramírez et al. 2012), although the higher effective temperature can also contribute.

6. Discussion

The mechanisms responsible for the frequency shifts of the acoustic oscillations during the solar magnetic activity cycle are

---

[3] The GSSP package is available for download at `https://fys.kuleuven.be/ster/meetings/binary-2015/gssp-software-package`

[4] In this work, we used the standard definitions: [X/Y] = log($N_{\rm X}/N_{\rm Y}$) − log($N_{\rm X}/N_{\rm Y}$)$_\odot$, and $A_{\rm X}$ = log ($N_{\rm X}/N_{\rm H}$) + 12, where $N_{\rm X}$ is the number density of element X in the stellar photosphere.
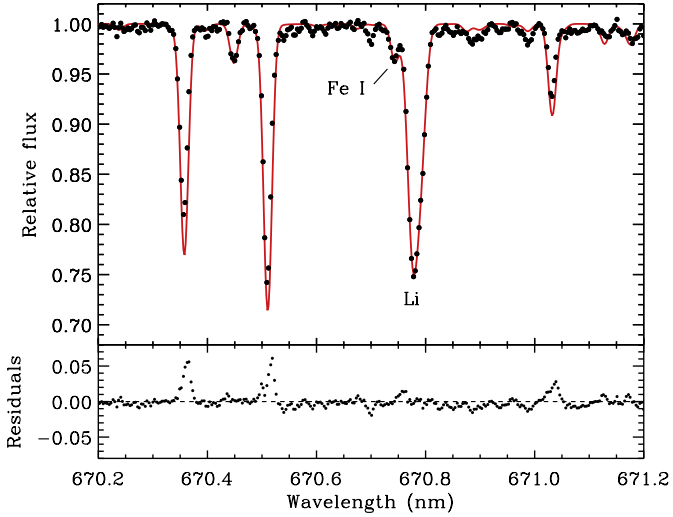
Fig. 7. *Top panel*: Lithium doublet of the solar analog KIC 10644253 observed with the HERMES instrument (dots) around 670.7 nm and associated spectral synthesis (red solid line) calculated using the spectroscopic set of atmospheric parameters given in Table 5. *Bottom panel*: residuals between the observed and the synthetic spectra.

Fig. 8. Dimensionless normalized $l = 1$ frequency shifts $(I_{nl}/I_{max}) \times \delta\nu_{nl}/\nu_{nl} \times \nu_{max}$ as a function of ν/ν_{max} for both the Sun (black squares) and KIC 10644253 (red dots). The solid lines correspond to the associated weighted linear regressions of the form $A_0\nu^2$.

still not completely clear. As shown by Libbrecht & Woodard (1990) for *p*-modes at intermediate angular degree, the *l*-dependence of the shifts can be largely eliminated by considering changes normalized with the mode inertia, $I_{nl} \times \delta\nu_{nl}$. This indicates that the direct mechanism responsible for the shifts is located close to the solar surface. Moreover, they showed that the frequency dependence of the shifts was flattened once it was normalized by the mode inertia as well. A decrease of less than 2% in the radial component of the turbulent velocity in the outer layers is assumed to explain the frequency increase of the low- and intermediate-degree acoustic modes with solar magnetic activity (Kuhn & Schüssler 2000; Dziembowski et al. 2001; Dziembowski & Goode 2005).

The dimensionless normalized frequency shifts defined as $(I_{nl}/I_{max}) \times \delta\nu_{nl}/\nu_{nl} \times \nu_{max}$ are shown in Fig. 8 as a function of ν/ν_{max} for both the Sun (Salabert et al. 2015) and KIC 10644253. The frequency ν_{max} at the maximum oscillation power was used because it is linearly related to the acoustic cut-off frequency (Belkacem et al. 2011). We only considered here the $l = 1$ modes as explained in Sect. 4. The solid lines correspond to weighted linear regressions of the form $A_0\nu^2$, where A_0 is the fitted value of the frequency shift at ν_{max}. The frequency dependence was assumed to follow the simple prescription by Gough (1990). We found $A_0 = 0.23 \pm 0.03$ μHz for the Sun and $A_0 = 0.26 \pm 0.10$ μHz for KIC 10644253. The A_0 value for KIC 10644253 at ν_{max} is compared to the observed frequency dependence of the $l = 1$ modes shown in Fig. 4. The measured frequency shifts for the Sun and the solar analog KIC 10644253 have a comparable frequency dependence as seen in Fig. 8. However, the theoretical predictions, such as the ones proposed by Chaplin et al. (2007b) and Metcalfe et al. (2007), suggest a slightly higher value for KIC 10644253 than for the Sun. But given the approximations considered in their theoretical estimations and the uncertainties on the extracted frequency shifts, both observations and predictions are consistent.

The frequency shifts measured in this work are clearly associated to the ~1.5-yr magnetic modulation observed in the photometric activity proxy S_{ph}. When compared to the Sun, the physical mechanism for these shifts could be related either to
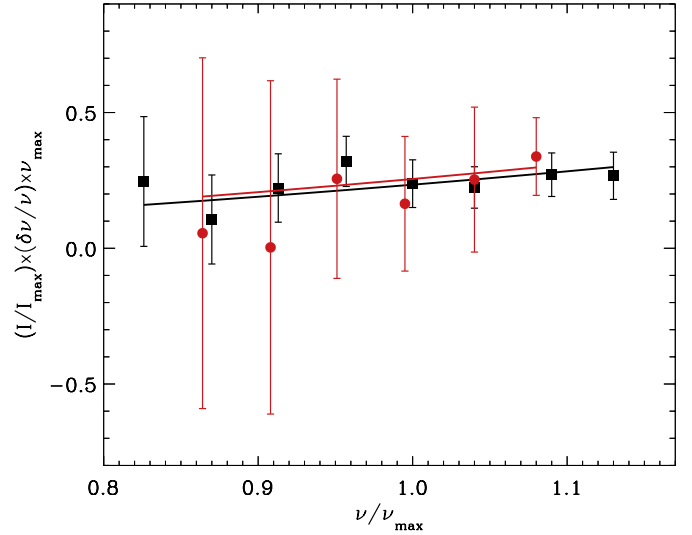
a long-period variation over a decade or so or to a short-period variation such as the QBO. This question is relevant since, as already mentioned, Egeland et al. (2015) report dual modulations of about 1.7 and 12 yr in the young solar analog HD 30495, which is a very similar object to KIC 10644253 in many ways. Moreover, the differences measured in the frequency shifts of the Sun during the 11-yr cycle and the QBO can be attributed to differences in the structure changes induced by the magnetic activity (Broomhall et al. 2012; Salabert et al. 2015). Indeed, the degree and frequency dependence of the solar frequency shifts were observed to be different for the QBO and the 11-yr cycle.

The larger frequency shifts of the QBO measured for the quadripolar $l = 2$ modes (Broomhall et al. 2012) were explained to be associated with an equatorial and deeper concentration of the structural changes in the QBO, as also suggested by Ulrich & Tran (2013) and McIntosh et al. (2015). Furthermore, KIC 10644253 is likely to have a very inclined rotation axis (see Table 1), although we cannot be more precise since the differences between the measurements exceed their reported uncertainties. The projected velocity $v \sin i$ of 1 km s^{-1} measured here with HERMES (Table 5) returns an angle of about 11°, confirming nonetheless the high inclination angle of this star in relation of the line of sight. The contribution of the zonal modes will then be smaller, so that a weaker degree dependence than for the Sun is expected for KIC 10644253. Moreover, based on Broomhall et al. (2012), the dimensionless frequency shifts of the solar QBO calculated as in Fig. 8 suggests that their frequency dependence is negligible. The slope of the frequency shifts measured in KIC 10644253 are similar to the one observed during the solar 11-yr cycle of the Sun, although the large errors prevent excluding a flatter slope, hence a deeper location of the source like in the QBO. We note as well that as a consequence of the highly inclined rotation axis of KIC 10644253, the activity proxy S_{ph} derived here should be considered as a lower limit of its photospheric activity.

7. Conclusions

We analyzed the photometric *Kepler* observations of the young (1 Gyr-old) solar analog KIC 10644253, collected in both long

and short cadences. We studied its temporal magnetic variability by estimating different proxies of activity. The light curve was directly analyzed to estimate the photometric activity through the measurement of the proxy S_{ph} over subseries of $5 \times P_{rot} = 54.55$ days. In addition, the temporal variability of the oscillation frequencies of the low-degree acoustic modes was obtained through the analysis of consecutive 180-day power spectra using peak-fitting and cross-correlation independent methods, and the associated frequency shifts $\langle \delta \nu \rangle$ were extracted. We showed that both the photometric activity proxy S_{ph} and the frequency shifts $\langle \delta \nu \rangle$ present the signature of magnetic activity with a significant temporal variability. Furthermore, a modulation of about 1.5 yr over the duration of the *Kepler* observations was measured in both observables of about 900 ppm for S_{ph} and 0.5 μHz for the frequency shifts. This 1.5-yr variation could actually be the signature of the short-period modulation, or quasi-biennal oscillation, of its magnetic activity as observed in the Sun (see, e.g., Fletcher et al. 2010) and the 1-Gyr-old solar analog HD 30495 with very close stellar properties (Egeland et al. 2015). Moreover, the comparison between the magnitude and the frequency dependence of the frequency shifts measured for KIC 10644253 with the ones obtained for the Sun indicates that the same physical mechanisms are involved in the subsurface inner layers in both stars.

In addition, complementary high-resolution spectroscopic observations of KIC 10644253 were collected by the HERMES instrument mounted on the 1.2 m *Mercator* telescope located in La Palma (Canary Islands, Spain). The analysis of the emission in the cores of the CaII H&K lines showed that KIC 10644253 is about 20% chromospherically more active than the mean emission of the Sun with an S index calibrated into the Mount Wilson Observatory system of 0.219 ± 0.014, thus confirming that it is an active object. Moreover, the high lithium abundance of 2.74 ± 0.03 dex and the effective temperature of 6006 ± 100 K of the solar analog KIC 10644253 mean that the lithium at the surface has not been depleted yet by internal processes (Ramírez et al. 2012). This is thus validating its young age (~1 Gyr-old) estimated from seismology and in agreement with a rotation period of about 11 days from gyrochronology (Meibom et al. 2011).

Finally, the young solar analog KIC 10644253 has been put on a long-term monitoring program with the HERMES spectrograph, which will provide measurements of the chromospheric S index over a long period of time. Moreover, new photometric observations in the near future with the Transiting Exoplanet Survey Satellite (TESS) instrument (Ricker et al. 2015) scheduled to be launched around 2017–2018 should again allow a monitoring of the photospheric activity of this star. That will provide a longer temporal coverage of KIC 10644253's activity, allowing us to compare it in greater detail with the Sun and HD 30495.

References

Aigrain, S., Llama, J., Ceillier, T., et al. 2015, MNRAS, 450, 3211
Anders, E., & Grevesse, N. 1989, Geochim. Cosmochim. Acta, 53, 197
Appourchaux, T., Chaplin, W. J., García, R. A., et al. 2012, A&A, 543, A54
Baglin, A., Michel, E., Auvergne, M., & The COROT Team 2006, in Proc. SOHO 18/GONG 2006/HELAS I, Beyond the spherical Sun, eds. K. Fletcher, & M. Thompson (Noordwijk), ESA SP, 624, 34
Baliunas, S. L., & Vaughan, A. H. 1985, ARA&A, 23, 379
Baliunas, S. L., Donahue, R. A., Soon, W. H. et al. 1995, ApJ, 438, 269
Ballot, J., Barban, C., & van't Veer-Menneret, C. 2011a, A&A, 531, A124
Ballot, J., Gizon, L., Samadi, R., et al. 2011b, A&A, 530, A97
Basu, S., Broomhall, A.-M., Chaplin, W. J., & Elsworth, Y. 2012, ApJ, 758, 43
Bazilevskaya, G., Broomhall, A.-M., Elsworth, Y., & Nakariakov, V. M. 2014, Space Sci. Rev., 186, 359
Beck, P. G., Allende Prieto, C., Van Reeth, T. et al. 2016, A&A, 589, A27
Belkacem, K., Goupil, M. J., Dupret, M. A., et al. 2011, A&A, 530, A142
Böhm-Vitense, E. 2007, ApJ, 657, 486
Bonanno, A., Fröhlich, H.-E., Karoff, C., et al. 2014a, A&A, 569, A113
Bonanno, A., Corsaro, E., & Karoff, C. 2014b, A&A, 571, A35
Borucki, W. J., Koch, D., Basri, G., et al. 2010, Science, 327, 977
Broomhall, A.-M., Chaplin, W. J., Elsworth, Y., & Simoniello, R. 2012, MNRAS, 420, 1405
Bruntt, H., Basu, S., Smalley, B., et al. 2012, MNRAS, 423, 122
Chaplin, W. J., Elsworth, Y., Isaak, G. R., et al. 1998, MNRAS, 300, 1077
Chaplin, W. J., Elsworth, Y., Isaak, G. R., Miller, B. A., & New, R. 2000, MNRAS, 313, 32
Chaplin, W. J., Elsworth, Y., Miller, B. A., Verner, G. A., & New, R. 2007a, ApJ, 659, 1749
Chaplin, W. J., Elsworth, Y., Houdek, G., & New, R. 2007b, MNRAS, 377, 17
Chaplin, W. J., Bedding, T. R., Bonanno, A., et al. 2011, ApJ, 732, L5
Chaplin, W. J., Basu, S., Huber, D., et al. 2014, ApJS, 210, 1
Domingo, V., Fleck, B., & Poland, A. I. 1995, Sol. Phys., 162, 1
do Nascimento, J.-D., Jr., Takeda, Y., Meléndez, J., et al. 2013, ApJ, 771, L31
Doyle, A. P., Davies, G. R., Smalley, B., Chaplin, W. J., & Elsworth, Y. 2014, MNRAS, 444, 3592
Duncan, D. K., Vaughan, A. H., Wilson, O. C., et al. 1991, ApJS, 76, 383
Dziembowski, W. A., Goode, P. R., & Schou, J. 2001, ApJ, 553, 897
Dziembowski, W. A., & Goode, P. R. 2005, ApJ, 625, 548
Egeland, R., Metcalfe, T. S., Hall, J. C., & Henry, G. W. 2015, ApJ, 812, 12
Fares, R., Donati, J.-F., Moutou, C., et al. 2009, MNRAS, 398, 1383
Fletcher, S. T., Broomhall, A.-M., Salabert, D., et al. 2010, ApJ, 718, L19
Fossat, E., Gelly, B., Grec, G., & Pomerantz, M. 1987, A&A, 177, L47
Frasca, A., Fröhlich, H.-E., Bonanno, A., et al. 2011, A&A, 532, A81
Fröhlich, C., Romero, J., Roth, H., et al. 1995, Sol. Phys., 162, 101
Fröhlich, H.-E., Frasca, A., Catanzaro, G., et al. 2012, A&A, 543, A146
García, R. A., Mathur, S., Salabert, D., et al. 2010, Science, 329, 1032
García, R. A., Hekker, S., Stello, D., et al. 2011, MNRAS, 414, L6
García, R. A., Ceillier, T., Salabert, D., et al. 2014a, A&A, 572, A34
García, R. A., Mathur, S., Pires, S., et al. 2014b, A&A, 568, A10
Gaulme, P., Appourchaux, T., & Boumier, P. 2009, A&A, 506, 7
Gelly, B., Lazrek, M., Grec, G., et al. 2002, A&A, 394, 285
Ghezzi, L., Cunha, K., Smith, V. V., et al. 2009, ApJ, 698, 451
Gough, D. O. 1990, Progress of Seismology of the Sun and Stars, 367, 283
Hall, J. C., Lockwood, G. W., & Skiff, B. A. 2007, AJ, 133, 862
Høg, E., Fabricius, C., Makarov, V. V., et al. 2000, A&A, 355, L27
Howe, R., Komm, R. W., & Hill, F. 2002, ApJ, 580, 1172
Jiménez-Reyes, S. J., García, R. A., Chaplin, W. J., & Korzennik, S. G. 2004, ApJ, 610, L65
Kuhn, J. R. 1988, ApJ, 331, L131
Kuhn, J. R., & Schüssler, M. 2000, Space Sci. Rev., 94, 177
Kurucz, R. L. 1993, Kurucz CD-ROM (Cambridge, MA: Smithsonian Astrophysical Observatory), December 4
Lanza, A. F., Das Chagas, M. L., & De Medeiros, J. R. 2014, A&A, 564, A50
Lehmann, H., Tkachenko, A., Semaan, T., et al. 2011, A&A, 526, A124
Libbrecht, K. G., & Woodard, M. F. 1990, Nature, 345, 779
Mathur, S., García, R. A., Régulo, C., et al. 2010, A&A, 511, A46
Mathur, S., García, R. A., Ballot, J., et al. 2014a, A&A, 562, A124
Mathur, S., Salabert, D., García, R. A., & Ceillier, T. 2014b, J. Space Weather and Space Climate, 4, 15
Marsden, S. C., Petit, P., Jeffers, S. V., et al. 2014, MNRAS, 444, 3517

McIntosh, S. W., Leamon, R. J., Krista, L. D., et al. 2015, Nat. Comms., 6, 6491
Meibom, S., Barnes, S. A., Latham, D. W., et al. 2011, ApJ, 733, L9
Metcalfe, T. S., Dziembowski, W. A., Judge, P. G., & Snow, M. 2007, MNRAS, 379, L16
Metcalfe, T. S., Basu, S., Henry, T. J., et al. 2010, ApJ, 723, L213
Metcalfe, T. S., Buccino, A. P., Brown, B. P., et al. 2013, ApJ, 763, L26
Metcalfe, T. S., Creevey, O. L., Doğan, G., et al. 2014, ApJS, 214, 27
Molenda-Żakowicz, J., Sousa, S. G., Frasca, A., et al. 2013, MNRAS, 434, 1422
Morgenthaler, A., Petit, P., Morin, J., et al. 2011, Astron. Nachr., 332, 866
Mosser, B., Michel, E., Appourchaux, T., et al. 2009, A&A, 506, 33
Noyes, R. W., Hartmann, L. W., Baliunas, S. L., Duncan, D. K., & Vaughan, A. H. 1984, ApJ, 279, 763
Oláh, K., Kolláth, Z., Granzer, T., et al. 2009, A&A, 501, 703
Pallé, P. L., Régulo, C., & Roca Cortés, T. 1989, A&A, 224, 253
Pinsonneault, M. H., Molenda-Żakowicz, J., et al. 2012, ApJS, 199, 30
Pires, S., Mathur, S., García, R. A., et al. 2015, A&A, 574, A18
Ramírez, I., Fish, J. R., Lambert, D. L., & Allende Prieto, C. 2012, ApJ, 756, 46
Raskin, G. 2011, Ph.D. Thesis, Katholieke Universiteit Leuven
Raskin, G., van Winckel, H., Hensberge, H., et al. 2011, A&A, 526, A69
Régulo, C., García, R. A., & Ballot, J. 2016, A&A, 589, A103
Ricker, G. R., Winn, J. N., Vanderspek, R., et al. 2015, J. Astron. Telescopes, Instruments, and Systems, 1, 014003
Saar, S. H., & Brandenburg, A. 1999, ApJ, 524, 295

Salabert, D., & Jiménez-Reyes, S. J. 2006, ApJ, 650, 451
Salabert, D., Fossat, E., Gelly, B., et al. 2004, A&A, 413, 1135
Salabert, D., García, R. A., Pallé, P. L., & Jiménez-Reyes, S. J. 2009, A&A, 504, L1
Salabert, D., Régulo, C., Ballot, J., García, R. A., & Mathur, S. 2011, A&A, 530, A127
Salabert, D., García, R. A., & Jiménez, A. 2013, Fifty Years of Seismology of the Sun and Stars, 478, 145
Salabert, D., García, R. A., & Turck-Chièze, S. 2015, A&A, 578, A137
Salabert, D., García, R. A., Beck, P. G., et al. 2016, A&A, submitted
Shulyak, D., Tsymbal, V., Ryabchikova, T., Stütz, C., & Weiss, W. W. 2004, A&A, 428, 993
Simoniello, R., Jain, K., Tripathy, S. C., et al. 2013, ApJ, 765, 100
Sneden, C. 1973, ApJ, 184, 839
Soderblom, D. R., Fedele, S. B., Jones, B. F., Stauffer, J. R., & Prosser, C. F. 1993, AJ, 106, 1080
Tkachenko, A. 2015, A&A, 581, A129
Tkachenko, A., Lehmann, H., Smalley, B., Debosscher, J., & Aerts, C. 2012, MNRAS, 422, 2960
Tsymbal, V. 1996, M.A.S.S., Model Atmospheres and Spectrum Synthesis, ASP Conf. Ser., 108, 198
Ulrich, R. K., & Tran, T. 2013, ApJ, 768, 189
Wilson, O. C. 1978, ApJ, 226, 379
Woodard, M. F., & Noyes, R. W. 1985, Nature, 318, 449